

1 **La Niña-like mean-state response to global warming**
2 **and potential oceanic roles**

3 Tsubasa Kohyama*, Dennis L. Hartmann, and David S. Battisti

4 *Department of Atmospheric Sciences, University of Washington, Seattle, Washington*

5 **Corresponding author address:* Department of Atmospheric Sciences, University of Washington,
6 Box 351640, Seattle, WA 98195-1640
7 E-mail: kohyama@uw.edu

ABSTRACT

8 The majority of the models that participated in the Coupled Model Inter-
9 comparison Project Phase 5 global warming experiments warm faster in the
10 eastern equatorial Pacific Ocean than the west. GFDL-ESM2M is an excep-
11 tion among the state-of-the-art global climate models in that the equatorial Pa-
12 cific sea surface temperature (SST) in the west warms faster than in the east.
13 In this model, the Walker circulation strengthens in response to warming, and
14 the centennial changes of the teleconnection patterns exhibit some common
15 features with those of observed interannual La Niña events. This study shows
16 that this La Niña-like trend may be an equally reasonable response to warming
17 by comparing the physical mechanisms in GFDL-ESM2M to other models.
18 GFDL-ESM2G, which differs from GFDL-ESM2M only in the oceanic com-
19 ponents yet warms without a clear zonal SST gradient, and HadGEM2-CC,
20 which exhibits a warming pattern that resembles the multi-model mean, are
21 used to explore some potentially important oceanic mechanisms. A robust ob-
22 served correlation between the zonal SST gradient and the amplitude of the El
23 Niño Southern Oscillation (ENSO) is reproduced well by GFDL-ESM2M but
24 not by the other two models. Considering that the ENSO amplitude in GFDL-
25 ESM2M is significantly suppressed by warming, the weakening ENSO am-
26 plitude may be causally related to its La Niña-like mean-state warming trend.
27 The most important physical difference between GFDL-ESM2M and GFDL-
28 ESM2G for ENSO appears to be that GFDL-ESM2M has larger diffusivity
29 and weaker stratification in the upper ocean.

30 **1. Introduction**

31 The tropical Pacific Ocean has profound impacts on the global climate system, and the response
32 of this region to anthropogenic greenhouse gas forcing has been a controversial research topic
33 since late 20th century (e.g., Knutson and Manabe 1995; Cane et al. 1997; Collins et al. 2005,
34 2010; Xie et al. 2010). The recent multi-decadal trends of the zonal sea surface temperature (SST)
35 gradient along the equator and its projection under global warming have received particular atten-
36 tion because of its potential impacts on the extratropical weather and climate (e.g., Christensen
37 et al. 2013). The projected influence is not limited to mean-state land temperature and precipita-
38 tion changes, but also extends to many other climatological elements, such as frequency of tropical
39 cyclone genesis over the central North Pacific (Yokoi and Takayabu 2009) and Antarctic sea ice
40 trends (e.g., Kohyama and Hartmann 2016).

41 In this study, we hereafter call a warming pattern “El Niño-like” (“La Niña-like”) when the east
42 (west) equatorial Pacific warms faster than the west (east) equatorial Pacific. Many studies inten-
43 tionally avoid these terms, which are associated with the El Niño Southern Oscillation (ENSO),
44 because “a reduction in the strength of the equatorial Pacific trade winds is not necessarily accom-
45 panied by a reduction in the magnitude of the east-west gradient of SST” as explained by Collins
46 et al. (2010). Other studies, however, continue to use ENSO terminology to characterize the struc-
47 ture of global change (e.g., Held et al. 2010; An et al. 2012) presumably because no other simple,
48 lucid way to describe them has been proposed. We have decided to follow the latter, but we shall
49 use these terms carefully in the sense that ENSO is an interannual climate mode that modulates
50 anomalies from the mean state, and that it is not necessarily controlled by the factors that control
51 changes in the mean state under greenhouse warming.

52 The majority of the models that participated in the Coupled Model Intercomparison Project
53 Phase 3 (CMIP3) and Phase 5 (CMIP5) exhibit El Niño-like SST trends, and therefore, the multi-
54 model mean SST trend pattern is also El Niño-like as schematically shown by Collins et al. (2010)
55 and calculated using CMIP5 model outputs by Ying et al. (2016). This SST trend pattern is highly
56 associated with the weakening Walker circulation as explained by Held and Soden (2006) and
57 Vecchi and Soden (2007) from the perspective of the global hydrological cycle. In agreement
58 with this, some studies reported that the observed sea-level pressure gradient along the equatorial
59 Pacific has been reduced during the past century (e.g., Vecchi et al. 2006; Zhang and Song 2006;
60 Tokinaga et al. 2012a). Some observational SST datasets support this standpoint (Fig. 1a, right).

61 Other observational SST datasets suggest, on the contrary, that the zonal SST gradient along
62 the equator has increased during the past century (Fig. 1a, left). Some studies based on observed
63 sea-level pressure trends (e.g., L'Heureux et al. 2013) and paleoproxies (e.g., An et al. 2012)
64 support this evidence as well. The observational uncertainty of the SST and sea-level pressure
65 trends mostly comes from limited data sampling, changing measurement techniques, and different
66 analysis procedures (Christensen et al. 2013). Though we have better datasets for the satellite era
67 that also show a clear La Niña-like trend (not shown), we cannot determine, based on the short time
68 span (1979-2015), whether the trend is purely unforced natural multi-decadal variability or partly
69 a forced response to anthropogenic climate change. Some model-based studies convincingly show
70 that the fast response to global warming should be La Niña-like and the slow response should be
71 El Niño-like (Held et al. 2010; An et al. 2012; Xiang et al. 2014), but this hypothesis has also been
72 difficult to test using observations.

73 The scientific question we address in this paper is whether a reasonable explanation can be given
74 to support the notion that the forced response of the mean-state equatorial Pacific to greenhouse
75 warming may actually be La Niña-like. Some earlier studies at the end of the last century showed

76 that the global warming trend should be associated with a La Niña-like SST trend because of
77 a so-called “ocean dynamical thermostat” mechanism (Clement et al. 1996; Cane et al. 1997).
78 This mechanism, however, was simulated by the Cane-Zebiak model (Zebiak and Cane 1987),
79 which assumes that the temperature of the climatological upwelling water in the eastern equatorial
80 Pacific remains fixed as a boundary condition under global warming. This assumption is now
81 thought to be a crucial problem, and after this, La Niña-like SST trends associated with global
82 warming has been largely unexplored using state-of-the-art global climate models (GCM) or Earth
83 system models (ESM). This question is still potentially interesting in the sense that, if the warming
84 response is La Niña-like, the recent robust Pacific SST trend during the satellite era (e.g., England
85 et al. 2014) could be understood partly as a forced response rather than purely as multi-decadal
86 variability.

87 In this regard, an interesting member of the CMIP5 model ensemble is GFDL-ESM2M model
88 (hereafter “M model”) in that it produces a well-defined La Niña-like response under both the rep-
89 resentative concentration pathways (RCP) 6.0 and 8.5 global warming scenarios (Fig. 1b). Many
90 studies have shown that the ENSO representation of the M model is reasonable (e.g., Bellenger
91 et al. 2014). The Geophysical Fluid Dynamics Laboratory (GFDL) also developed GFDL-ESM2G
92 model (hereafter “G model”), which differs from the M model only in its oceanic components
93 (Dunne et al. 2012, 2013), and this model does not show a clear La Niña-like response (Fig.
94 3c). Therefore, we hope to identify some important oceanic responses to warming that determine
95 whether the forced responses simulated by these models will be El Niño-like or La Niña-like.

96 In this study, our main focus is to compare the M and G model, and also HadGEM2-CC model
97 (hereafter “Had model”) that exhibits similar SST trends to the multi-model mean El Niño-like
98 pattern (Fig. 3c), to shed light on the possibility of La Niña-like mean-state warming. It is a hard
99 task to determine whether the M model captures the real world better than the other models, but

100 even if its response to warming turns out to be unrealistic, investigating model differences should
101 help us understand the climate system better.

102 This article is organized as follows. The data used in this study are described in the next section.
103 In section 3, we describe the time evolution of the zonal SST gradient simulated by the three
104 models and associated atmospheric changes to confirm the importance of the differences. Then, in
105 section 4, we show a difference in capability of the models to simulate a robust observed constraint
106 between the zonal SST gradient and the ENSO amplitude. In section 5, we discuss some possible
107 mechanisms whereby the ocean might cause the difference in the climatology and the warming
108 response. Summary and discussion are given in section 6.

109 **2. Data and Methods**

110 The observed monthly SST data used in this study are from the Hadley Centre Sea Ice
111 and Sea Surface Temperature (HadISST) (Rayner et al. 2003) available online at [http://](http://www.metoffice.gov.uk/hadobs/hadisst/index.html)
112 www.metoffice.gov.uk/hadobs/hadisst/index.html and the National Oceanic and Atmo-
113 spheric Administration (NOAA) Extended Reconstructed Sea Surface Temperature V3b (ERSST
114 V3b) (Smith et al. 2008) available online at [http://www.esrl.noaa.gov/psd/data/gridded/](http://www.esrl.noaa.gov/psd/data/gridded/data.noaa.ersst.html)
115 [data.noaa.ersst.html](http://www.esrl.noaa.gov/psd/data/gridded/data.noaa.ersst.html) for the time span from 1870 through 2015. For more recent years
116 (1979-2015), we also use the reanalysis monthly temperature (SST and 2 meter temperature)
117 from the European Centre for Medium-Range Weather Forecasts (ECMWF) ERA Interim Re-
118 analysis data (Dee et al. 2011) available online at [http://apps.ecmwf.int/datasets/data/](http://apps.ecmwf.int/datasets/data/interim-full-moda/levtype=sfc/)
119 [interim-full-moda/levtype=sfc/](http://apps.ecmwf.int/datasets/data/interim-full-moda/levtype=sfc/). The horizontal resolution is 1 degree for HadISST and
120 ERA Interim, and 2 degrees for ERSST V3b in both zonal and meridional direction. We have
121 also used the ERA Interim data for zonal wind and vertical motion from 1979 through 2012 with
122 3-degree, monthly resolution for the 1000-100 hPa layer.

123 The model output of the surface temperature, zonal wind, atmospheric vertical motion, precip-
124 itation, oceanic potential temperature, and oceanic vertical heat diffusivity are from the CMIP5
125 data (Taylor et al. 2012) available at the websites of GFDL Data Portal (<http://nomads.gfdl.noaa.gov:8080/DataPortal/cmip5.jsp>) and Program for Climate Model Diagnosis and In-
126 tercomparison (<https://pcmdi.llnl.gov/projects/cmip5/>). We mainly use the output from
127 the M, G, and Had models, but we have also used the data from MIROC5 and GFDL-CM3 for
128 the last section. The experiments considered in this study are the first ensemble member of the
129 RCP 6.0 and RCP 8.5 runs from 2006 through 2100 except for the vertical heat diffusivity, which
130 is archived in the form of monthly climatology derived from the historical run (1986-2005). In
131 addition, we also refer to SST from 4,000 year-long pre-industrial control run of GFDL CM2.1
132 (Delworth et al. 2006; Wittenberg et al. 2006).

134 All the analysis methods used in this study are simple regression, correlation, and compositing
135 analyses. When we estimate degrees of freedom in the data for statistical tests, we use a formula
136 given by Bretherton et al. (1999) to take autocorrelations into account. Then, to calculate the
137 estimated range of a true correlation, we use Fisher's transformation.

138 **3. Time evolution of the zonal SST gradient and atmospheric circulation change**

139 Our first goal is to describe how SST trends evolve in the three models under the RCP 8.5
140 scenario and to confirm the importance of the difference. For the latter, we particularly focus
141 on the Walker circulation change and the resulting land temperature and precipitation changes to
142 illustrate potential societal implications.

143 *a. Time evolution of the zonal SST gradient*

144 Figure 2 shows the spatial patterns of the bidecadal mean SST* (hereafter “*” denotes “devia-
145 tions from the global mean”) starting from 2016, 2036, 2056, and 2076 expressed with respect to
146 the decadal mean starting from 2006. Even in the first bidecade, a hint of difference in the zonal
147 SST gradient is already apparent, especially between the M and Had models. Then, after half a
148 century, the three models start to show their distinct spatial structures. The last bidecadal patterns
149 are essentially the same as those introduced in Fig. 1. This temporal evolution confirms that the
150 trend patterns shown in the introduction section are not due to influences of a few extreme events
151 in a relatively short time span but due to a gradual process during this century.

152 An interesting difference in the North Pacific SST trend also appears. In the M model, the
153 SST warming off the North American west coast is relatively weak compared to the center of
154 North Pacific. This feature is not apparent in the G and Had models. This anomalous SST pat-
155 tern in the M model looks like the so-called “Blob” mode (e.g., Hartmann 2015), which is known
156 to have become the second most important mode of global SST variability during the satellite
157 era and to have evolved into an extreme event with more than 2 standard deviations in 2014
158 winter. According to Hartmann (2015) and Watson et al. (2016) (see also a submitted paper
159 by Seager and Henderson available at [http://ocp.ldeo.columbia.edu/res/div/ocp/pub/
160 seager/Seager_Henderson_ridge.pdf](http://ocp.ldeo.columbia.edu/res/div/ocp/pub/seager/Seager_Henderson_ridge.pdf)), it is virtually certain that the Blob is a forced response
161 to the tropical west Pacific warm anomalies through atmospheric teleconnection, so the fact that
162 the Blob mode emerges in the M model is consistent with the dominance of west Pacific warm
163 anomaly.

164 *b. The Walker circulation change*

165 Next, we investigate the response of the Walker circulation to warming in each model. Figure 3
166 shows the equatorial meridional-mean warming response of zonal wind and vertical motion in the
167 three models. As many previous articles have suggested (e.g., Tokinaga et al. 2012b), the Walker
168 circulation weakens as the SST experiences El Niño-like warming in the Had model. By contrast,
169 in the M model, the Walker circulation strengthens as the SST experiences La Niña-like warming.
170 The G model also shows a qualitatively similar strengthening, but the signal is much weaker as the
171 SST trend does not exhibit a clear La Nina-like pattern. Also shown in the top panels are those of
172 the observed trends during the satellite era. Though there is no reason to assume that the satellite
173 era is an analog for global warming, the remarkable resemblance in Walker circulation change
174 between observations and the M model increases the interest in comparing these models.

175 One might wonder how to reconcile the strengthening Walker circulation in the M model with
176 the robust conclusion from the energy and water balances that the atmospheric circulation should
177 weaken under global warming (Held and Soden 2006). It is important, however, to remember
178 that this explanation only constrains the global mean change. The scatter plots in Fig. 4 show the
179 relationship between the annual-mean temperature change and the precipitation increase expressed
180 with respect to the mean over 2006-2015. Also shown are the least-square best fit line of the
181 precipitation increase and the estimated increase of water vapor due to the Clausius-Clapeyron
182 relationship ($7\%/K$) assuming that the relative humidity remains constant. The explanation given
183 by Held and Soden (2006) was that, to increase precipitation more slowly than $7\%/K$, the water
184 vapor increase has to be compensated by weakening atmospheric circulation. In the majority of
185 global climate models including the M and Had models, this is true for the global mean circulation
186 as shown in Fig. 4 (a). The problem is that many previous studies extrapolated this explanation

187 to circulations in narrower regions, such as the Walker circulation, where this assumption is not
188 always true because of lateral transport processes (Fig. 4b). Therefore, the strengthening Walker
189 circulation in the M model does not violate the conclusion derived from the global energy and
190 water balances.

191 *c. Land temperature and precipitation change*

192 Figure 5 (a) shows the difference of the land temperature response to warming between the
193 Had model (El Niño-like) and the M model (La Niña-like) in December-January-February (DJF).
194 To suppress the polar amplification signals, the zonal mean response is removed beforehand. Also
195 shown is an observational map of the detrended DJF land temperature regressed onto the detrended
196 SST anomalies averaged over the Niño3 region (5N-5S, 150W-90W) during the satellite era. These
197 two maps suggest that the global warming response to the tropical Pacific SST resembles the
198 interannual ENSO teleconnection to first order. One major difference is seen in Australia, but this
199 could be an artifact of taking out the zonal mean response, which is presumably influenced by the
200 strong warm anomalies in South America.

201 Precipitation* change in North America also exhibits different precipitation patterns between
202 the two models (Fig. 5b). Particularly, at least in the RCP 8.5 run, the La Niña-like model (i.e., M
203 model) simulates significantly drier climate in Gulf States at the 95% confidence level, whereas
204 the El Niño-like model (i.e., Had model) simulates the reverse. This feature is also known to
205 be typical for the interannual ENSO mode. Figure 5 is a good indication that the difference in
206 the Pacific SST trends are potentially important for climate change over land, and particularly so
207 for North America. The trend differences in Fig. 5 are significant, but the natural year-to-year
208 variability is also large.

209 **4. A robust observed constraint between the zonal SST gradient and the ENSO amplitude** 210 **and its reproducibility by the models**

211 In this section, we first show that an interesting feature of the M model is that the ENSO ampli-
212 tude is significantly suppressed under greenhouse warming. Then, we explore some implications
213 of the weakening amplitude trends for the mean-state zonal SST gradient, referencing a robust
214 constraint that exists in observations and the M model but not in the G and Had models.

215 Figure 6 (a) shows the 3-year running standard deviation (RSTD) of the regional mean SST
216 anomalies in the Niño3 region for the M, G, and Had models (RCP 8.5). The RSTD does not
217 significantly change during the century in the G and Had model at the 95% confidence level,
218 but it exhibits a significant decrease in the M model. To show that this amplitude decrease is
219 unlikely to be a result of natural variability, we have also performed the same analysis using the
220 first 2000 years of the 4,000 year-long pre-industrial control run of GFDL CM2.1. Specifically,
221 we have calculated the significance of the amplitude trends for every possible time span with
222 length of 95 years (i.e., Year 2-96, 3-97, ..., and 1904-1999, starting from Year 2 because we
223 calculate 3-year RSTD). Surprisingly, out of the two millennia, only 3 eras (i.e., 8 time spans
224 starting from 125-128, 297-299, and 1716) have experienced significant amplitude decrease at the
225 95% confidence level. In addition, none of them has shown a steeper trend than the RCP 8.5 run
226 of the M model. Though GFDL CM2.1 is a different model from the M model, it is reasonably
227 similar in many respects (Dunne et al. 2012) including the strengthening Walker circulation in
228 response to warming (Tanaka et al. 2005). Therefore, to the best of our knowledge, it is very
229 unlikely that the significant amplitude decrease shown in the M model is due to centennial natural
230 variability, and we have good statistical evidence to hypothesize that the ENSO amplitude in the
231 M model is suppressed as a forced response to warming.

232 Next, Fig. 6 (b) suggest that the large ENSO events in the M model are mostly El Niño, rather
233 than La Niña, which reflects the skewed probability density function of ENSO in the M model.
234 For reference, the skewnesses of annual-mean detrended Niño3 regional-mean SST anomalies are
235 0.34 for observations (satellite era), 0.30 for the M model, 0.36 for the G model, and -0.29 for the
236 Had model (RCP 8.5), where positive skewness denotes that El Niño events tend to be stronger
237 than La Niña events. This nonlinearity of ENSO motivates us to look at the relationship between
238 the ENSO amplitude and the mean state. If ENSO becomes inactive in response to warming,
239 fewer extreme ENSO events will occur, which means fewer strong El Niño events because of the
240 nonlinearity in this model. Therefore, the mean state is expected to become La Niña-like (see
241 also a submitted paper by Atwood et al. available at [http://www.atmos.washington.edu/
242 ~david/Atwood_et_al_ENSO_submitted_2016.pdf](http://www.atmos.washington.edu/~david/Atwood_et_al_ENSO_submitted_2016.pdf)). Conversely, the La Niña-like mean state
243 might also influence the weakening ENSO amplitude as discussed in many previous studies (e.g.,
244 Collins et al. 2010; Kim et al. 2011). One mechanism in particular links weaker stratification of
245 the ocean to SST that is less responsive to wind anomalies.

246 Figure 7 (a) shows the observed relationship between the standardized RSTD and the zonal SST
247 gradient (ZSG) index. Here, the ZSG index is defined as Niño3 minus Niño4 regional-mean SST
248 anomalies, so that positive (negative) ZSG means El Niño-like (La Niña-like) mean state. The
249 observed RSTD and ZSG indices, especially during the satellite era, exhibit a remarkably high
250 correlation with statistical significance at the 95% confidence level, which supports the idea of in-
251 teractions between mean-state and amplitude mentioned in the previous paragraph. In other words,
252 a La Niña-like mean-state and inactive ENSO tend to coexist, and vice versa. The lag-correlation
253 property between the two indices is also shown in the right panels, but the lag-correlation coeffi-
254 cients with positive and negative lags are not well-separated in terms of the estimated range of the

255 true correlations at the 95% confidence level. This means we cannot determine the direction of
256 causality based on the statistics for this length of integration.

257 Figure 7 (b) and (c) show the same correlation properties but for the three models. Interestingly,
258 the M model reproduces the simultaneous and lagged correlations in both RCP 6.0 and 8.5 runs,
259 but those of the G and Had models are insignificant at the 95% confidence level. Because the
260 typical period of the interannual ENSO mode is 3-5 years, one may be skeptical about the sensi-
261 tivity of these correlations to the length of the time window for calculating the RSTD and ZSG
262 indices. Figure 8 shows the results of the same analysis but for 7-year and 11-year running stan-
263 dard deviation and mean. Notwithstanding the strong autocorrelations of the time series, the two
264 indices in the M model exhibit statistically significant correlations at the 95% confidence level,
265 and do not depend on the length of the window. In addition, the La Niña-like trend in the RCP
266 8.5 simulations is mostly explained by the linear relationship with the RSTD index in both 7-year
267 and 11-year windows, which implies the importance of the ENSO amplitude change in relation to
268 the mean state trends. In the observations, however, the 11-year window is too strong a low-pass
269 filter to retain enough degrees of freedom for the correlation to be statistically significant at the
270 95% confidence level. Nevertheless, the insignificance of the correlation mostly emanates from
271 the pre-satellite era for which we do not have high-quality datasets.

272 Though the feature discussed above is not enough to conclude that the M model simulates the
273 zonal SST gradient more realistically, it lends confidence to the notion that the La Niña-like warm-
274 ing scenario may be as reasonable as the El Niño-like warming scenario, since consistent physical
275 mechanisms can be outlined. Considering the fact that the previous studies have not reached con-
276 sensus on how the ENSO amplitude will change under global warming (Collins et al. 2010), a
277 more La Niña-like mean-state with warming remains a plausible outcome.

278 **5. Discussion on hypothetical physical mechanisms to yield the inter-model differences**

279 Three possible causal relationships among the greenhouse forcing, the mean-state change, and
280 the amplitude change are summarized in Fig. 9. These involve the direction of causality between
281 the zonal SST gradient, ENSO amplitude, and greenhouse gas warming. Though it is not clear
282 which causal relationship in Fig. 9 is the most important one, we have enough evidence to assume
283 that some important oceanic mechanisms control the zonal SST gradient response to warming,
284 because the M and G models are different only in their oceanic components. In this section, we
285 list some potentially important mechanisms for simulating the La Niña-like warming pattern in
286 the M model, based on the different configurations and features of the two models.

287 *a. Potential roles of equatorial diffusivity and thermal stratification*

288 One of the major climatological differences in the equatorial Pacific between the M and G mod-
289 els is the strength of the vertical heat diffusivity. Figure 10 (a) shows the vertical heat diffusivity
290 of the two models. The vertical heat diffusivity of the M model is about an order of magnitude
291 larger than that of the G model in the upper ocean. Previous studies show that small diffusivity
292 tends to yield large ENSO amplitudes (Meehl et al. 2001), and GFDL scientists also learned from
293 experience that the exceedingly small equatorial diffusivities in the G model increased the ENSO
294 variance (Matthew Harrison, personal communication). Therefore, we could argue that the larger
295 diffusivity of the M model might make ENSO anomalies easier to reduce under warming climate
296 than those in the G model. This is a possible explanation that causes ENSO amplitudes in the M
297 model to be more suppressed under warming, which can then yield La Niña-like warming.

298 Another related equatorial property is thermal stratification. Figure 10 (b) shows the difference
299 of the climatological thermal stratification in the eastern equatorial Pacific between the M and G
300 models, and between the M and Had models. The weak eastern equatorial thermal stratification in

301 the M model can directly influence the mean-state zonal SST gradient even without the help of the
302 suppressed ENSO amplitude. For example, if the thermal stratification is weaker, it is harder to
303 warm up Niño3 SST given the same heat input. The weaker thermal stratification would also cause
304 Niño3 SST to be less sensitive to the weakening trade winds as a response to warming, because of
305 anomalously warmer upwelling water.

306 *b. Potential mechanism related to the strength of the polar amplification*

307 From a more global perspective, the strength of the polar amplification of global warming may
308 also affect the warming response of the zonal SST gradient. Figure 11 (a) shows the difference
309 map of the trends of SST* between the M and G models and that of the M and Had models. These
310 maps show that polar amplification is weaker in the M model, especially in the eastern Pacific
311 basin. This might then cause the eastern equatorial Pacific upwelling water to be anomalously
312 cold, because the outcrops of isopycnal surfaces from which the upwelling water originates are
313 generally observed at higher latitudes. This is another possible mechanism to obtain the La Niña-
314 like trend in this model.

315 We are, however, more skeptical about this view than about the equatorial upper oceanic prop-
316 erties, because oceanic temperature anomalies in the 150-200 m layer do not exhibit any major
317 qualitative difference (Fig. 11b). If the oceanic transport from the origin of the equatorial up-
318 welling water is the most dominant cause, we expect major difference in the ocean interior just
319 like at the surface. We are also not certain about the time scale needed for changing the temper-
320 ature of the upwelling water. Therefore, the mid-latitude difference shown in Fig. 11 (a) may
321 be an effect of atmospheric teleconnections caused by the SST warming pattern in the equato-
322 rial Pacific. We could interpret the Northern-midlatitude pattern as the enhanced Blob mode, for
323 instance, which is perhaps a corollary of the La Niña-like warming.

324 **6. Summary and concluding remarks**

325 We have shown that GFDL-ESM2M (M model) is an interesting outlier in the CMIP5 mod-
326 els, because it exhibits a clear La Niña-like response to global warming in the equatorial Pacific.
327 GFDL-ESM2G (G model), which differs from the M model only in the oceanic components, does
328 not yield well-defined La Niña-like warming, however. Using this difference, we have explored
329 the potential oceanic roles that may be important for the difference in the trends of the zonal SST
330 gradient. We also compared the M model with HadGEM2-CC (Had model), which exhibits a
331 typical El Niño-like trend that resembles the multi-model mean response to warming.

332 First of all, in section 3, we have shown that the La Niña-like warming in the M model is a
333 gradual process that takes almost a full century to reach the mature phase. The Walker circulation
334 change associated with the La Niña-like response is similar to the observed change during the
335 satellite era, which is opposite to what the Had model and the multi-model mean project. Though
336 there is no reason to believe that the relatively short time span of the satellite era represents the
337 actual warming response, to determine whether the recent strengthening Walker circulation (e.g.,
338 England et al. 2014) is purely due to natural multi-decadal variability is a problem that deserves
339 careful investigation, because the Pacific zonal SST gradient change has very important impacts
340 on temperature and precipitation changes on land.

341 Therefore, in section 4, we have explored whether the La Niña-like trend in the M model is a
342 reasonable response to warming. Because the ENSO amplitude in this particular model exhibits
343 a significant decrease in the RCP 8.5 run, we have investigated whether this feature is related to
344 the change of the mean-state zonal SST gradient. Specifically, we have detected a robust observed
345 correlation between the zonal SST gradient and ENSO amplitude that is reproduced well by the M
346 model but not by the G and Had models. This high correlation can be physically understood with

347 multiple possible mechanisms. Because of the ENSO nonlinearity that exists in both observations
348 and the M model, the suppressed ENSO amplitude means less strong El Niño events, which leads
349 to La Niña-like mean state. On the other hand, a La Niña-like mean state enhances mean upwelling
350 and zonal advection, and weakens the thermal stratification, which might influence the ENSO
351 dynamics to suppress its amplitude. We could also argue that both the mean-state and the ENSO
352 amplitude might be independently forced by greenhouse warming. Since the research community
353 has yet to reach consensus on the ENSO amplitude trends, one of our important conclusions is that
354 La Niña-like response to global warming deserves more attention in future studies particularly in
355 the context of the climatological interactions between the mean-state and the ENSO amplitude and
356 their future changes.

357 In section 5, we have argued that differences in the oceanic model components could potentially
358 be important for this issue. Our main hypothesis is that, because the climatological diffusivity and
359 stratification in the M and G models are different, they might influence the response of the ENSO
360 dynamics to warming. For example, excessively small diffusivity in the G model tends to yield
361 large ENSO amplitudes, so the ENSO in this model may be harder to suppress than that in the
362 M model under warming. This would make the interaction between the ENSO amplitude and the
363 mean-state less tight, and therefore, it becomes less likely to yield the well-defined La Niña-like
364 warming as in the M model. On the other hand, the weaker climatological thermal stratification
365 in the M model may make the surface wind forcing less efficient in warming SST in the Niño 3
366 region. From a more global perspective, a potential implication of the weaker polar amplification
367 in the M model relating to the origin of the equatorial upwelling water has been discussed, but the
368 importance of this effect may be secondary. This is because the temperature response in the ocean
369 interior deeper than 150 m, which is the main trajectory from the extratropical isopycnal outcrop

370 to the Ekman upwelling region, does not exhibit a major qualitative difference among the three
371 models.

372 One important caveat of this study is that, to focus on the oceanic difference between the M and
373 G model, we have only used three models to do the analyses for this study. Therefore, we have not
374 discussed any potentially important difference in the atmospheric components of the models. To
375 simulate the La Niña-like trend, however, it is virtually certain that the role of the atmosphere is
376 as important as the role of the ocean. For instance, the strength of atmospheric damping feedback
377 (i.e., SST in a warmer climate yields stronger atmospheric damping, such as latent heat release and
378 radiation, which leads to smaller SST variance) could have an important influence on the trends of
379 the ENSO amplitude.

380 The capability of simulating the robust relationship between ENSO amplitude and zonal SST
381 gradient discussed in section 4 is not a sufficient condition to yield the La Niña-like response to
382 global warming. Preliminary analyses reveal that some CMIP5 models reproduce the observed
383 constraint between the zonal SST gradient and the ENSO amplitude, but nevertheless exhibit an
384 El Niño-like warming response. Figure 12 shows some results obtained from observations (1921-
385 2015), the M model, MIROC 5, and GFDL-CM3 (RCP 8.5) for the time series of Niño 3 and 4
386 indices (1st row), the running standard deviation and the zonal SST gradient indices (2nd row), the
387 lag correlations between them (3rd row), and the lag-regression maps of SST anomalies onto the
388 running standard deviation time series (bottom row). These results clearly show that many other
389 necessary conditions are required to realistically simulate eastern equatorial Pacific variability in
390 addition to the zonal SST gradient. MIROC 5, which exhibits El Niño-like warming, reproduces
391 the simultaneous and lag correlations between the zonal SST gradient and the ENSO amplitude,
392 but the ENSO in this model is too regular (i.e., periodic). GFDL-CM3, which does not yield a

393 clear trend in the zonal SST gradient, simulates realistic ENSO well, but the lag regression maps
394 look fairly different from observations.

395 We have also found that many other CMIP5 models do not yield high correlations between the
396 zonal SST gradient and the ENSO amplitude as observed in the real world. It is true that the vast
397 majority of the CMIP5 models and the multi-model mean exhibit El Niño-like response to global
398 warming, but the range of spatial patterns they produce is not consistent. Hence, we do not have
399 a lot of faith in the multi-model mean pattern of the mean-state SST warming. Considering its
400 challenge as a scientific problem and its societal importance, further studies on the possibility of
401 La Niña-like response are needed.

402 *Acknowledgments.* The work was supported by the National Science Foundation (NSF) under
403 Grant AGS-0960497 and the first author's work is also supported by NSF under Grant AGS-
404 1122989, Takenaka Scholarship Foundation, and Iizuka Takeshi Scholarship Foundation. We
405 would like to thank Casey Wall for correcting English grammar of the first draft, and Alyssa
406 Atwood for preprocessing the output from 4,000 year-long pre-industrial control run of GFDL
407 CM2.1. We are also grateful to Cecilia Bitz, Christopher Bretherton, Matthew Harrison, Isaac
408 Held, and Andrew Shao for their helpful comments and suggestions.

409 **References**

410 An, S.-I., J.-W. Kim, S.-H. Im, B.-M. Kim, and J.-H. Park, 2012: Recent and future sea surface
411 temperature trends in tropical Pacific warm pool and cold tongue regions. *Climate Dyn.*, **39** (6),
412 1373–1383.

413 Bellenger, H., É. Guilyardi, J. Leloup, M. Lengaigne, and J. Vialard, 2014: ENSO representation
414 in climate models: from CMIP3 to CMIP5. *Climate Dyn.*, **42** (7-8), 1999–2018.

415 Bretherton, C. S., M. Widmann, V. P. Dymnikov, J. M. Wallace, and I. Bladé, 1999: The effective
416 number of spatial degrees of freedom of a time-varying field. *J. Climate*, **12**, 1990–2009, doi:
417 10.1175/1520-0442(1999)012<1990:TENOSD>2.0.CO;2.

418 Cane, M. A., A. C. Clement, A. Kaplan, Y. Kushnir, D. Pozdnyakov, R. Seager, S. E. Zebiak, and
419 R. Murtugudde, 1997: Twentieth-century sea surface temperature trends. *Science*, **275 (5302)**,
420 957–960.

421 Christensen, J., and Coauthors, 2013: *Climate Phenomena and their Relevance for Future Re-*
422 *gional Climate Change*, book section 14, 1217–1308. Cambridge University Press, Cambridge,
423 United Kingdom and New York, NY, USA, doi:10.1017/CBO9781107415324.028.

424 Clement, A. C., R. Seager, M. A. Cane, and S. E. Zebiak, 1996: An ocean dynamical thermostat.
425 *J. Climate*, **9 (9)**, 2190–2196.

426 Collins, M., and Coauthors, 2005: El Niño-or La Niña-like climate change? *Climate Dyn.*, **24 (1)**,
427 89–104.

428 Collins, M., and Coauthors, 2010: The impact of global warming on the tropical Pacific Ocean
429 and El Niño. *Nature Geosci.*, **3 (6)**, 391–397.

430 Dee, D. P., and Coauthors, 2011: The ERA-interim reanalysis: configuration and performance of
431 the data assimilation system. *Quart. J. Roy. Meteor. Soc.*, **137**, 553–597, doi:10.1002/qj.828.

432 Delworth, T. L., and Coauthors, 2006: GFDL’s CM2 global coupled climate models. Part
433 I: Formulation and simulation characteristics. *Journal of Climate*, **19 (5)**, 643–674, doi:
434 10.1175/JCLI3629.1.

435 Dunne, J. P., and Coauthors, 2012: GFDL's ESM2 global coupled climate-carbon Earth System
436 Models. Part I: Physical formulation and baseline simulation characteristics. *J. Climate*, **25** (19),
437 6646–6665.

438 Dunne, J. P., and Coauthors, 2013: GFDL 's ESM2 global coupled climate–Carbon Earth System
439 Models. Part II: Carbon system formulation and baseline simulation characteristics. *J. Climate*,
440 **26** (7), 2247–2267.

441 England, M. H., and Coauthors, 2014: Recent intensification of wind-driven circulation in the
442 Pacific and the ongoing warming hiatus. *Nature Climate Change*, **4** (3), 222–227.

443 Hartmann, D. L., 2015: Pacific sea surface temperature and the winter of 2014. *Geophys. Res.*
444 *Lett.*, **42** (6), 1894–1902.

445 Held, I. M., and B. J. Soden, 2006: Robust responses of the hydrological cycle to global warming.
446 *J. Climate*, **19** (21), 5686–5699.

447 Held, I. M., M. Winton, K. Takahashi, T. Delworth, F. Zeng, and G. K. Vallis, 2010: Probing the
448 fast and slow components of global warming by returning abruptly to preindustrial forcing. *J.*
449 *Climate*, **23** (9), 2418–2427.

450 Kim, D., Y.-S. Jang, D.-H. Kim, Y.-H. Kim, M. Watanabe, F.-F. Jin, and J.-S. Kug, 2011: El Niño–
451 Southern Oscillation sensitivity to cumulus entrainment in a coupled general circulation model.
452 *J. Geophys. Res.*, **116** (D22).

453 Knutson, T. R., and S. Manabe, 1995: Time-mean response over the tropical Pacific to increased
454 CO₂ in a coupled ocean-atmosphere model. *J. Climate*, **8** (9), 2181–2199.

455 Kohyama, T., and D. L. Hartmann, 2016: Antarctic sea ice response to weather and climate modes
456 of variability. *J. Climate*, **29** (2), 721–741.

- 457 L'Heureux, M. L., S. Lee, and B. Lyon, 2013: Recent multidecadal strengthening of the Walker
458 circulation across the tropical Pacific. *Nature Climate Change*, **3** (6), 571–576.
- 459 Meehl, G., P. Gent, J. Arblaster, B. Otto-Bliesner, E. Brady, and A. Craig, 2001: Factors that affect
460 the amplitude of El Niño in global coupled climate models. *Climate Dyn.*, **17** (7), 515–526.
- 461 Rayner, N., D. E. Parker, E. Horton, C. Folland, L. Alexander, D. Rowell, E. Kent, and
462 A. Kaplan, 2003: Global analyses of sea surface temperature, sea ice, and night marine
463 air temperature since the late nineteenth century. *J. Geophys. Res.*, **108** (D14), 4407, doi:
464 10.1029/2002JD002670.
- 465 Smith, T. M., R. W. Reynolds, T. C. Peterson, and J. Lawrimore, 2008: Improvements to NOAA's
466 historical merged land-ocean surface temperature analysis (1880-2006). *J. Climate*, **21** (10),
467 2283–2296.
- 468 Tanaka, H. L., N. Ishizaki, and D. Nohara, 2005: Intercomparison of the intensities and trends of
469 Hadley, Walker and Monsoon circulations in the global warming projections. *SOLA*, **1**, 77–80,
470 doi:10.2151/sola.2005-021.
- 471 Taylor, K. E., R. J. Stouffer, and G. A. Meehl, 2012: An overview of CMIP5 and the experiment
472 design. *Bull. Amer. Meteor. Soc.*, **93** (4), 485–498.
- 473 Tokinaga, H., S.-P. Xie, A. Timmermann, S. McGregor, T. Ogata, H. Kubota, and Y. M. Oku-
474 mura, 2012a: Regional patterns of tropical Indo-Pacific climate change: evidence of the Walker
475 circulation weakening. *J. Climate*, **25** (5), 1689–1710.
- 476 Tokinaga, H., S.-P. Xie, C. Deser, Y. Kosaka, and Y. M. Okumura, 2012b: Slowdown of the Walker
477 circulation driven by tropical Indo-Pacific warming. *Nature*, **491** (7424), 439–443.

- 478 Vecchi, G. A., and B. J. Soden, 2007: Global warming and the weakening of the tropical circula-
479 tion. *J. Climate*, **20** (17), 4316–4340.
- 480 Vecchi, G. A., B. J. Soden, A. T. Wittenberg, I. M. Held, A. Leetmaa, and M. J. Harrison, 2006:
481 Weakening of tropical Pacific atmospheric circulation due to anthropogenic forcing. *Nature*,
482 **441** (7089), 73–76.
- 483 Watson, P. A. G., A. Weisheimer, J. R. Knight, and T. N. Palmer, 2016: The role of the tropi-
484 cal West Pacific in the extreme Northern Hemisphere winter of 2013/2014. *J. Geophys. Res.*,
485 **121** (4), 1698–1714, doi:10.1002/2015JD024048.
- 486 Wittenberg, A. T., A. Rosati, N.-C. Lau, and J. J. Ploshay, 2006: GFDL’s CM2 global coupled
487 climate models. Part III: Tropical Pacific climate and ENSO. *Journal of Climate*, **19** (5), 698–
488 722, doi:10.1175/JCLI3631.1.
- 489 Xiang, B., B. Wang, J. Li, M. Zhao, and J.-Y. Lee, 2014: Understanding the anthropogenically
490 forced change of equatorial Pacific trade winds in coupled climate models. *J. Climate*, **27** (22),
491 8510–8526.
- 492 Xie, S.-P., C. Deser, G. A. Vecchi, J. Ma, H. Teng, and A. T. Wittenberg, 2010: Global warming
493 pattern formation: sea surface temperature and rainfall. *J. Climate*, **23** (4), 966–986.
- 494 Ying, J., P. Huang, and R. Huang, 2016: Evaluating the formation mechanisms of the equatorial
495 Pacific SST warming pattern in CMIP5 models. *Adv. Atmos. Sci.*, **33** (4), 433–441.
- 496 Yokoi, S., and Y. N. Takayabu, 2009: Multi-model projection of global warming impact on tropical
497 cyclone genesis frequency over the western north pacific. *J. Meteor. Soc. Japan*, **87** (3), 525–
498 538, doi:10.2151/jmsj.87.525.

499 Zebiak, S. E., and M. A. Cane, 1987: A model El Niño-Southern Oscillation. *Mon. Wea. Rev.*,
500 **115 (10)**, 2262–2278.

501 Zhang, M., and H. Song, 2006: Evidence of deceleration of atmospheric vertical overturning
502 circulation over the tropical Pacific. *Geophys. Res. Lett.*, **33 (12)**.

503 **LIST OF FIGURES**

504 **Fig. 1.** (a): Observed sea surface temperature (SST) trends computed relative to the tropical Pacific
505 mean trends (30°S-30°N, 90°E-60°W) in two different datasets. Blue colors denote a warm-
506 ing slower than the tropical Pacific mean, not a cooling. Unit is K/100years. (b): As in (a),
507 but for the model output from GFDL-ESM2M in the RCP 6.0 and RCP 8.5 experiments.
508 (c): As in (b), but for GFDL-ESM2G and HadGEM2-CC under RCP 8.5. 27

509 **Fig. 2.** Left: Bidecadal mean SST* (“*” denotes “deviations from the global mean”) in GFDL-
510 ESM2M under RCP 8.5, starting from 2016, 2036, 2056, and 2076, computed relative to
511 the decadal mean SST* starting from 2006. Unit is K/100years. Middle: As in left, but for
512 GFDL-ESM2G. Right: As in left, but for HadGEM2-CC. 28

513 **Fig. 3.** Top left: Equatorial (10°S-10°N) meridional mean trends of zonal wind in the ERA-Interim
514 reanalysis data during the satellite era. Contour interval is 0.3 (m/s)/30years. Zero contours
515 are omitted, and positive (negative) anomalies are shaded orange (blue). Top right: As in top
516 left, but for vertical motion. Contour interval is 3 (mPa/s)/30years. 2nd row: As in top, but
517 for the epochal difference of 2070-2099 minus 2006-2035 in GFDL-ESM2M under RCP
518 8.5. Contour intervals are 0.2 m/s for zonal wind and 2 hPa/day for vertical motion. 3rd
519 row: As in the 2nd row, but for GFDL-ESM2G. Bottom row: As in the 2nd row, but for
520 HadGEM2-CC. 29

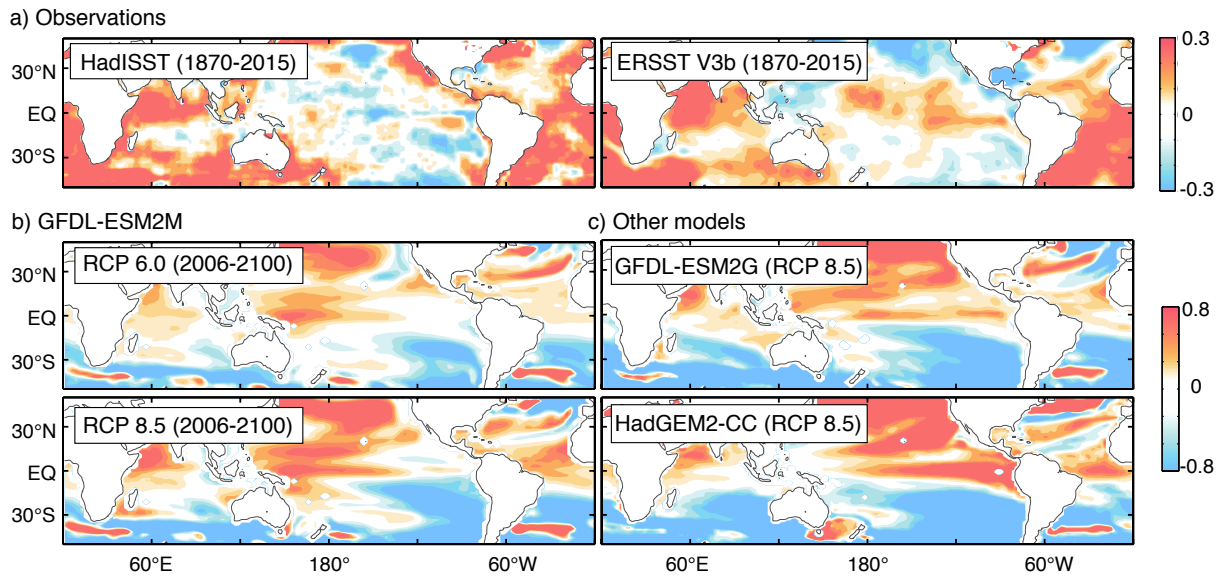
521 **Fig. 4.** (a): Scatter plots showing the relationship between the global mean surface temperature
522 change and the global precipitation change in two models under RCP 8.5. Each dot repre-
523 sents annual mean computed relative to the mean over 2006-2015. The least-square best fit
524 lines are shown in blue, and the estimated increase of water vapor due to Clausius-Clapeyron
525 relationship (7%/K) in red. (b): As in (a), but for the Pacific mean (90°S-90°N, 120°E-
526 80°W). 30

527 **Fig. 5.** (a): Left, Difference of the December-January-February (DJF) land surface temperature
528 trends between the two models under RCP 8.5. The trends are expressed with respect to the
529 zonal mean trends at each longitude so that the polar amplification signals are removed. Unit
530 is K/100years. Right, Regression map of DJF two meter temperature onto the Niño3 SST
531 anomalies in the ERA-Interim reanalysis data during the satellite era. Unit is K/K. (b): Left,
532 DJF precipitation trends in the two models expressed with respect to the global mean trends.
533 Unit is mm/day/100years. Right, DJF precipitation in the Gulf States in the two models
534 expressed with respect to the mean over 2006-2015. The dashed lines show the least-square
535 best fit lines, and the shaded areas show the estimated ranges of the true trends at the 95 %
536 confidence level. 31

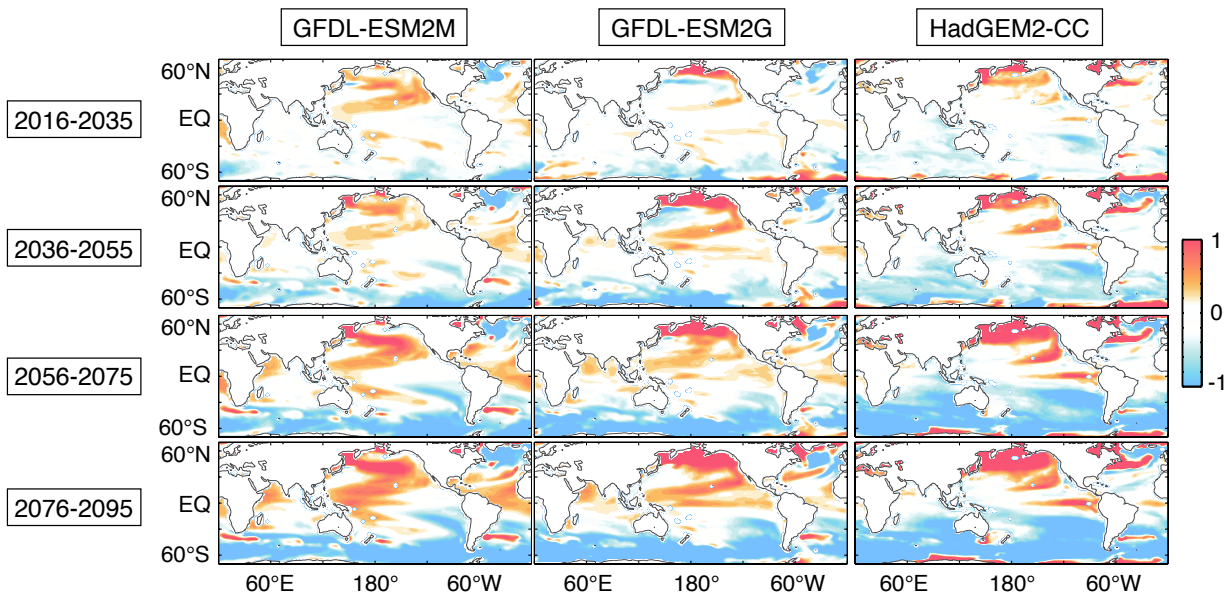
537 **Fig. 6.** (a): With-trend 3-year running standard deviations (RSTD) of the Niño3 SST anomalies in
538 the three models under RCP 8.5. The dashed lines show the least-square best fit lines, and
539 the shaded areas show the estimated ranges of the true trends at the 95% confidence level.
540 (b): Detrended annual mean Niño3 SST anomalies in the three models. 32

541 **Fig. 7.** (a): Left, Detrended 3-year RSTD of the observed Niño3 SST anomalies (blue) and the
542 zonal SST gradient (ZSG) index defined as 3-year running means of the Niño3 minus Niño4
543 SST anomalies (red). The results of HadISST (top) and ERA-Interim (bottom) are shown.
544 Right, Lag correlations between the two indices shown in the left panels. Error bars show
545 the estimated ranges of the true correlations at the 95 % confidence level. (b): As in (a),
546 but for GFDL-ESM2M under RCP 6.0 and 8.5. (c): As in (a), but for GFDL-ESM2G and
547 HadGEM2-CC under RCP 8.5. 33

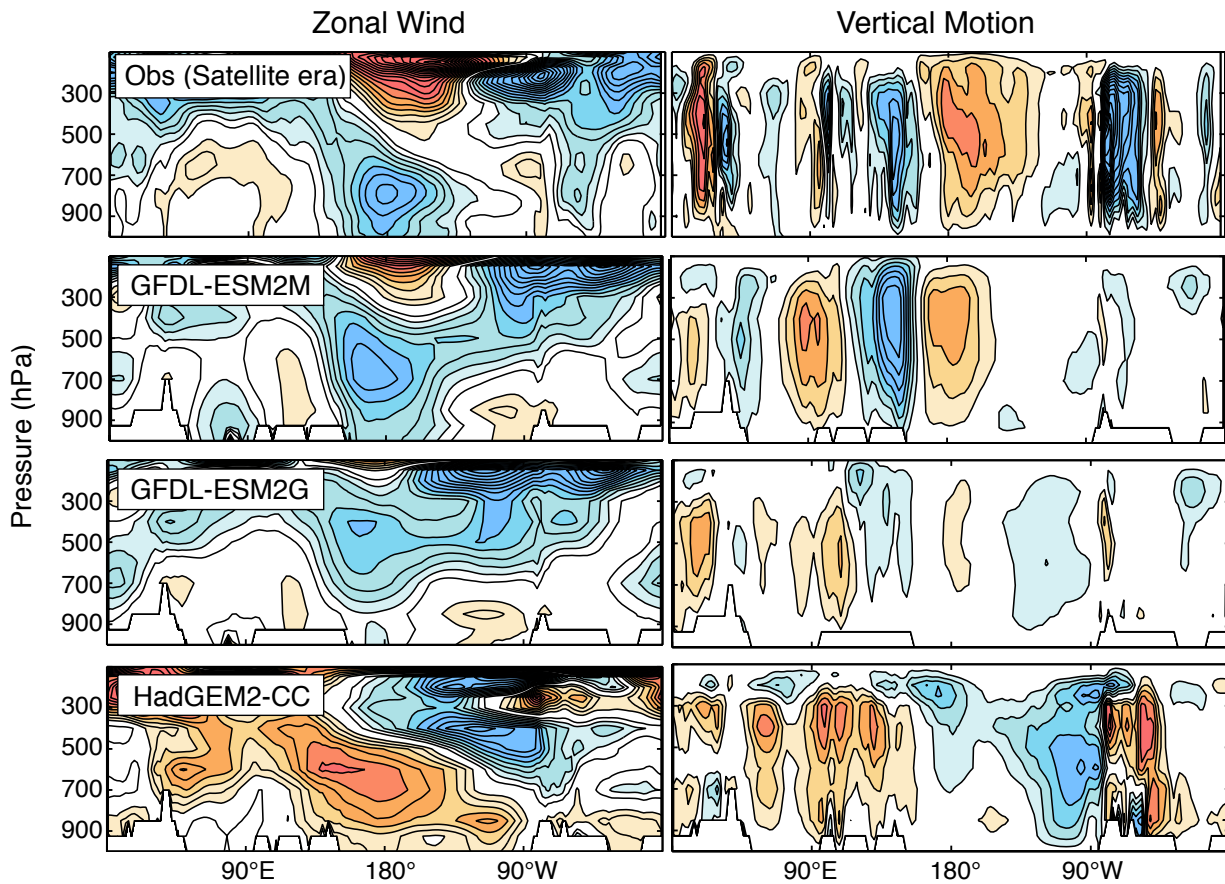
548	Fig. 8. (a): As in the left panels in Fig. 7, but the window length is 7 years. Only the results of HadISST and GFDL-ESM2M (RCP 6.0 and 8.5) are shown. Correlation coefficients are shown at the top right. For RCP 8.5, also shown is the same plot but for the with-trend indices. The dashed lines show the least-square best fit lines. (b): As in (a), but the window length is 11 years.	34
549		
550		
551		
552		
553	Fig. 9. Three possible causal relationships among greenhouse forcing, the ENSO amplitude change, and the La Niña-like mean-state response in GFDL-ESM2M.	35
554		
555	Fig. 10. (a): Climatology of the equatorial (5°S-5°N) vertical heat diffusivity in the two models derived from historical runs. Bold lines show 0.002 m ² /s, contour interval is 0.001 m ² /s, and higher diffusivity is shaded orange. (b): Difference of the climatological, equatorial thermal stratification between GFDL-ESM2M and the other two models derived from 2006-2035 in the RCP 8.5 runs. Bold lines show 0 /s, contour interval is 0.004 /s, and positive (negative) values are shaded orange (blue).	36
556		
557		
558		
559		
560		
561	Fig. 11. (a): Difference of the SST* warming response between GFDL-ESM2M and the other two models. The warming response is calculated as epochal difference of 2071-2100 minus 2006-2035. (b): As in Fig. 2, but for the vertical mean oceanic temperature within the 150-200 m layer.	37
562		
563		
564		
565	Fig. 12. (a): The annual mean Niño3 (blue) and Niño4 (red) SST anomalies expressed with respect to 1921-1930 (observations) or 2006-2015 (models). Observations are from HadISST, and the model outputs are derived from RCP 8.5. Dashed lines show the least-square best fit lines, and the shaded areas show the estimated ranges of the true trends. (b): As in the left panels in Fig. 7, but for observations and a different set of three models under RCP 8.5. The plots of observations and GFDL-ESM2M are identical as ones shown in Fig. 7. (c): As in (b), but for the right panels in Fig. 7. (d): Lag regression maps of detrended annual mean SST onto detrended 3-year RSTD of the Niño3 SST anomalies. Each row shows different lags. The positive lags denote that RSTD lags SST, and vice versa. Positive (negative) anomalies are shaded orange (blue).	38
566		
567		
568		
569		
570		
571		
572		
573		
574		



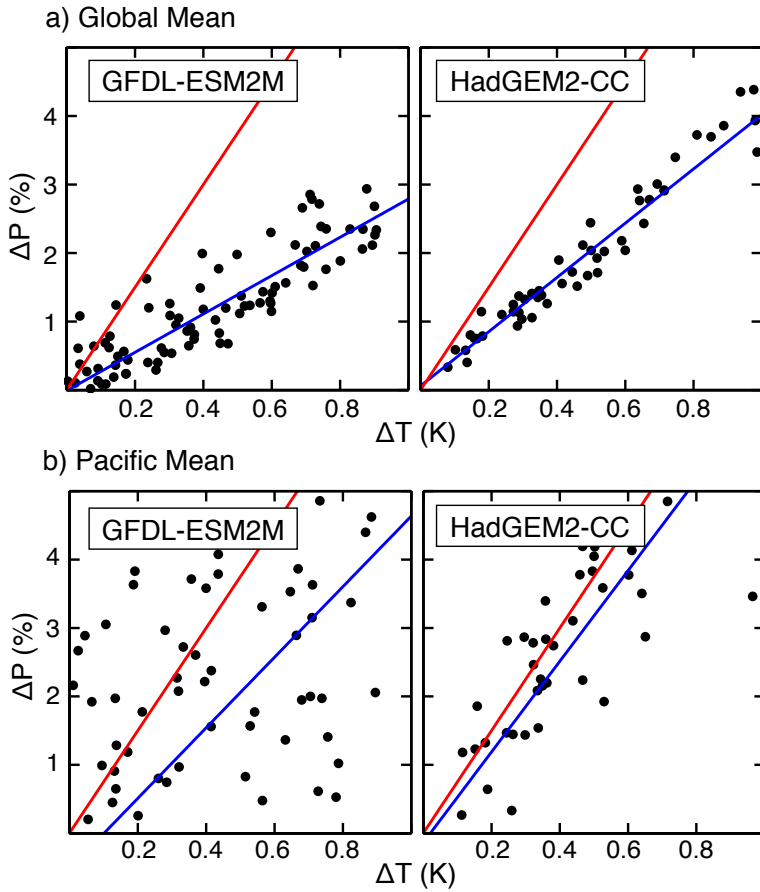
575 FIG. 1. (a): Observed sea surface temperature (SST) trends computed relative to the tropical Pacific mean
 576 trends (30°S-30°N, 90°E-60°W) in two different datasets. Blue colors denote a warming slower than the tropical
 577 Pacific mean, not a cooling. Unit is K/100years. (b): As in (a), but for the model output from GFDL-ESM2M
 578 in the RCP 6.0 and RCP 8.5 experiments. (c): As in (b), but for GFDL-ESM2G and HadGEM2-CC under RCP
 579 8.5.



580 FIG. 2. Left: Bidecadal mean SST* (“*” denotes “deviations from the global mean”) in GFDL-ESM2M under
 581 RCP 8.5, starting from 2016, 2036, 2056, and 2076, computed relative to the decadal mean SST* starting from
 582 2006. Unit is K/100years. Middle: As in left, but for GFDL-ESM2G. Right: As in left, but for HadGEM2-CC.

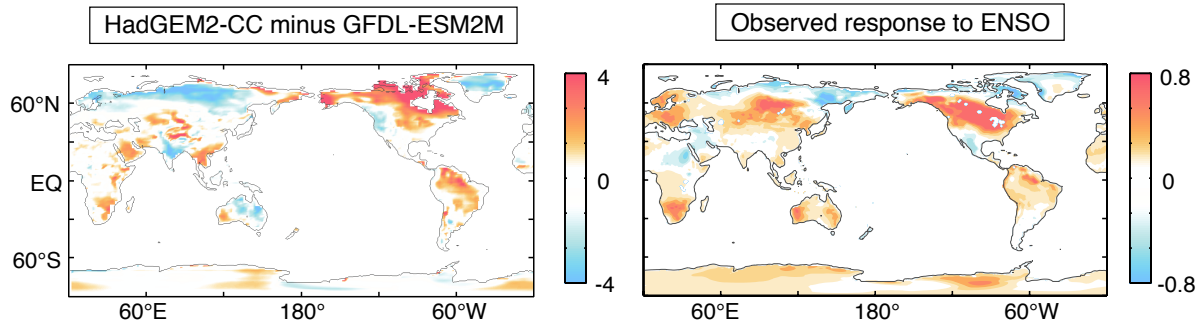


583 FIG. 3. Top left: Equatorial (10°S - 10°N) meridional mean trends of zonal wind in the ERA-Interim reanalysis
 584 data during the satellite era. Contour interval is $0.3 \text{ (m/s)}/30\text{years}$. Zero contours are omitted, and positive
 585 (negative) anomalies are shaded orange (blue). Top right: As in top left, but for vertical motion. Contour
 586 interval is $3 \text{ (mPa/s)}/30\text{years}$. 2nd row: As in top, but for the epochal difference of 2070-2099 minus 2006-2035
 587 in GFDL-ESM2M under RCP 8.5. Contour intervals are 0.2 m/s for zonal wind and 2 hPa/day for vertical
 588 motion. 3rd row: As in the 2nd row, but for GFDL-ESM2G. Bottom row: As in the 2nd row, but for HadGEM2-
 589 CC.

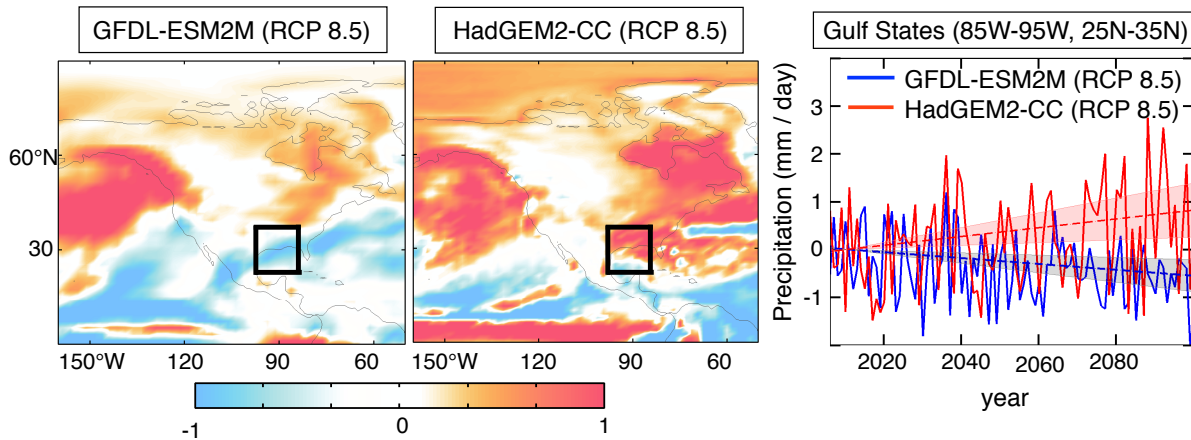


590 FIG. 4. (a): Scatter plots showing the relationship between the global mean surface temperature change and
 591 the global precipitation change in two models under RCP 8.5. Each dot represents annual mean computed
 592 relative to the mean over 2006-2015. The least-square best fit lines are shown in blue, and the estimated increase
 593 of water vapor due to Clausius-Clapeyron relationship (7%/K) in red. (b): As in (a), but for the Pacific mean
 594 (90°S-90°N, 120°E-80°W).

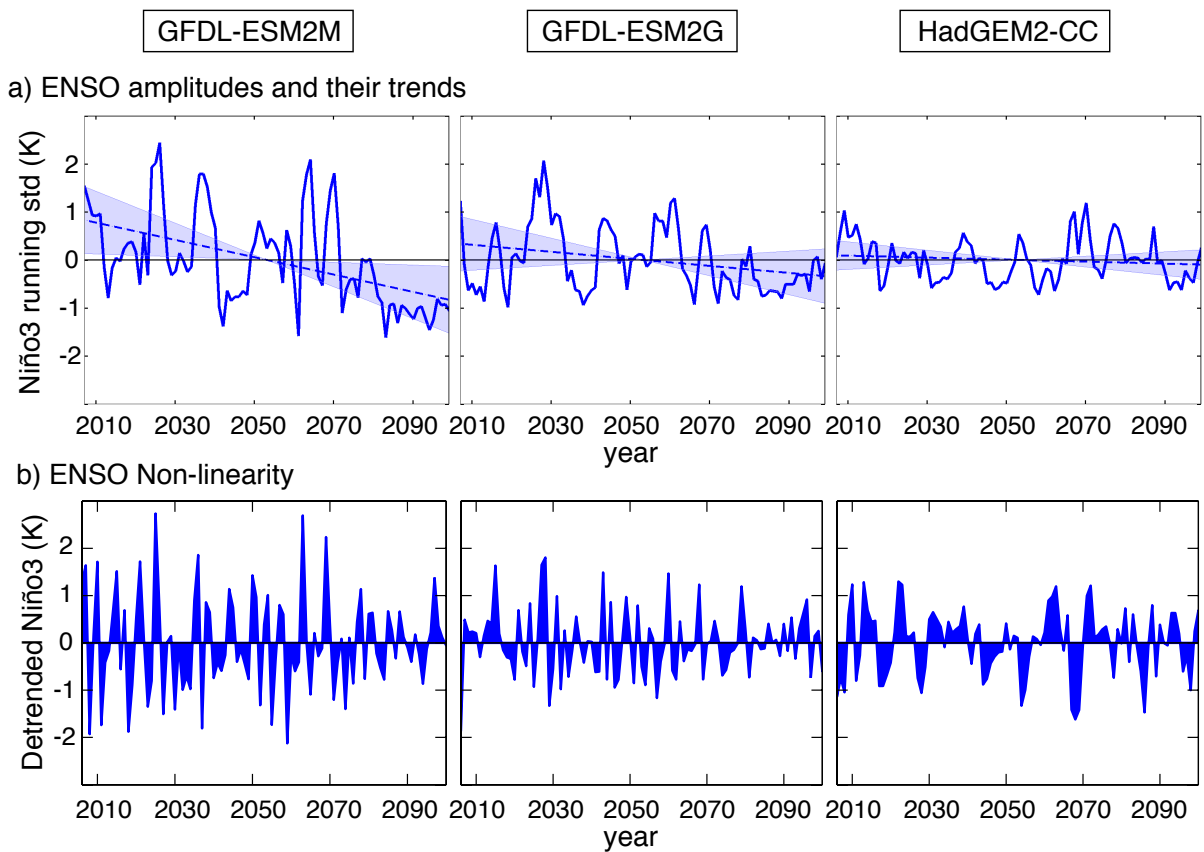
a) Land surface temperature response



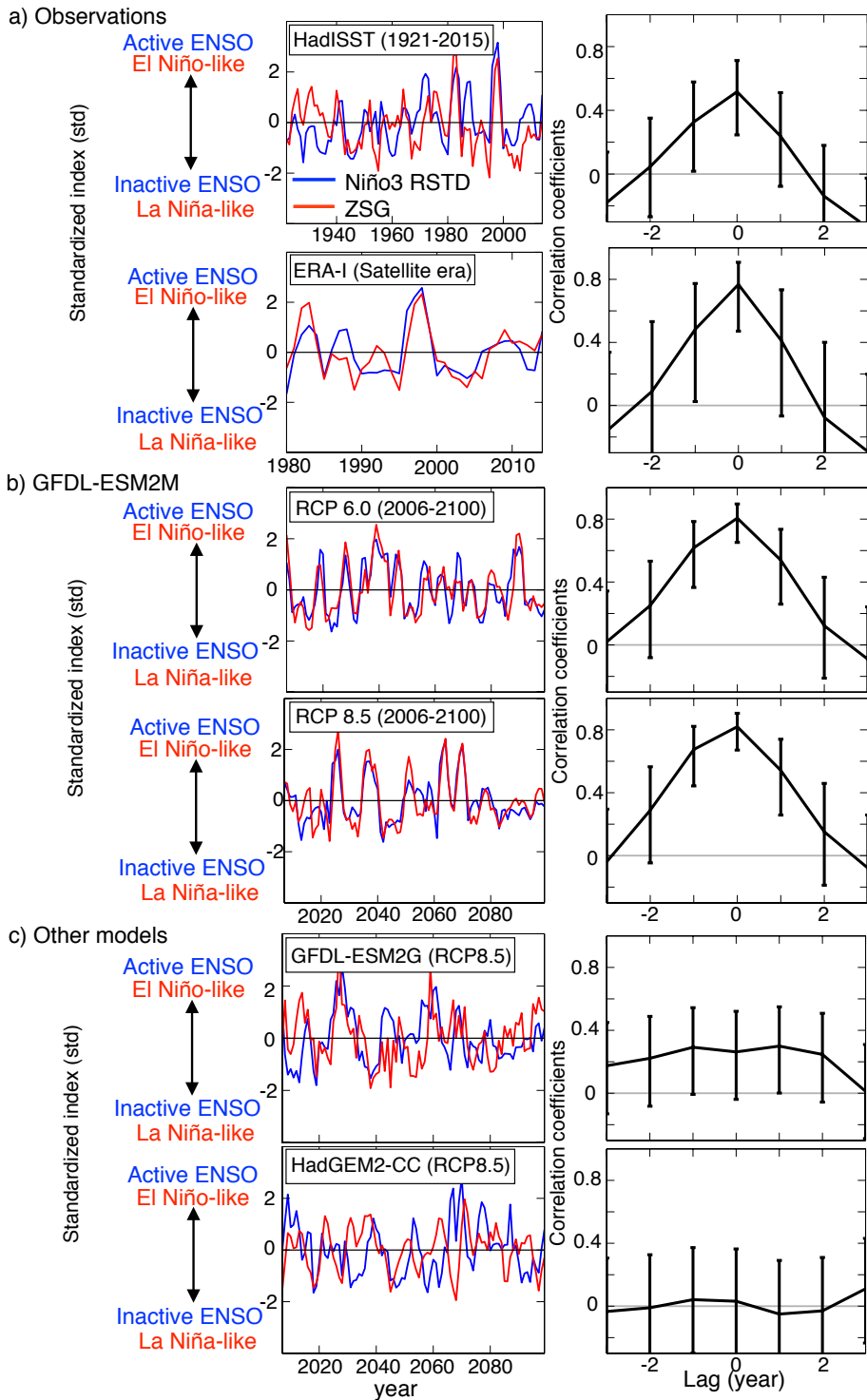
b) Precipitation response



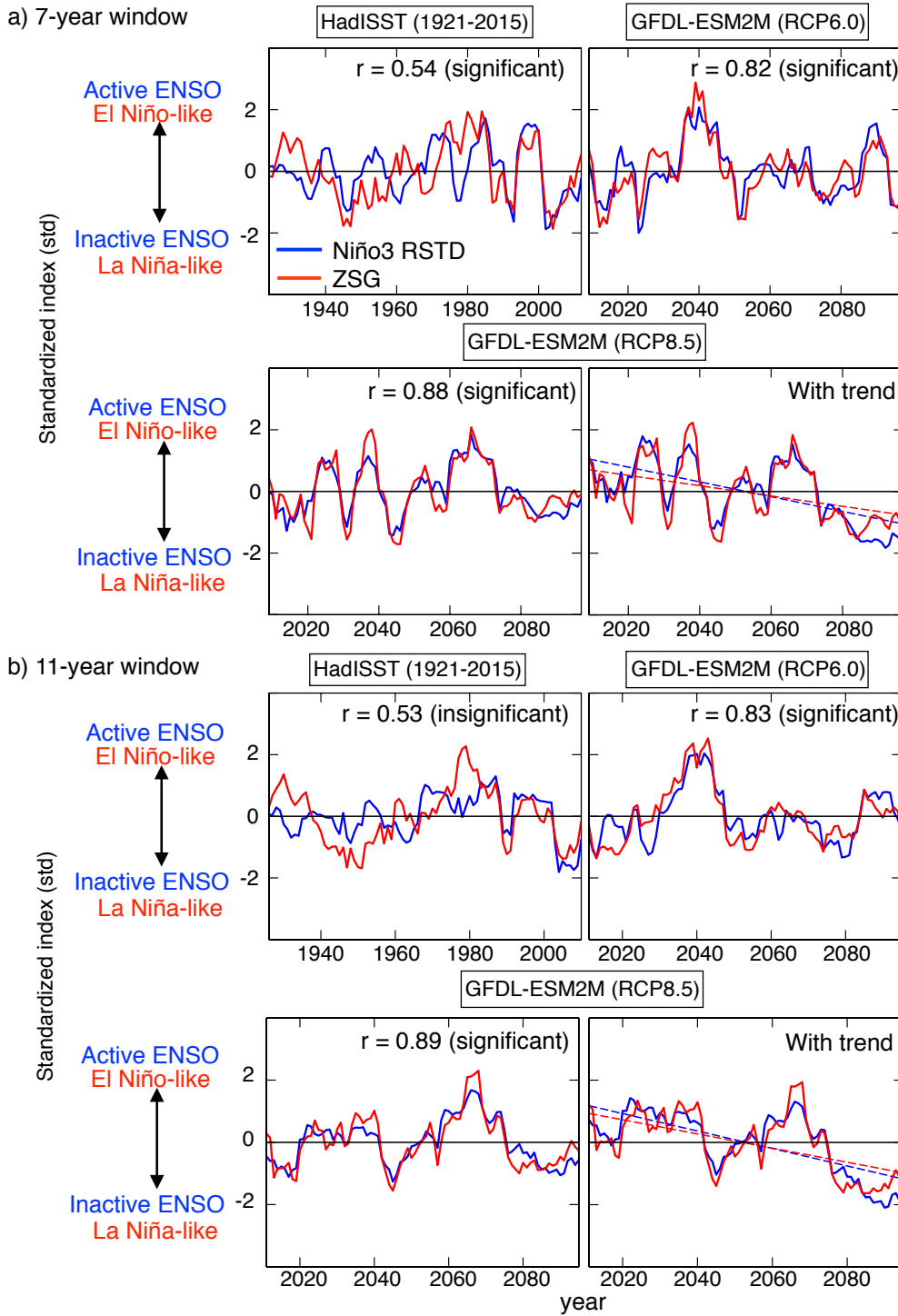
595 FIG. 5. (a): Left, Difference of the December-January-February (DJF) land surface temperature trends be-
 596 tween the two models under RCP 8.5. The trends are expressed with respect to the zonal mean trends at each
 597 longitude so that the polar amplification signals are removed. Unit is K/100years. Right, Regression map of DJF
 598 two meter temperature onto the Niño3 SST anomalies in the ERA-Interim reanalysis data during the satellite
 599 era. Unit is K/K. (b): Left, DJF precipitation trends in the two models expressed with respect to the global mean
 600 trends. Unit is mm/day/100years. Right, DJF precipitation in the Gulf States (location indicated in the left panel)
 601 in the two models expressed with respect to the mean over 2006-2015. The dashed lines show the least-square
 602 best fit lines, and the shaded areas show the estimated ranges of the true trends at the 95 % confidence level.



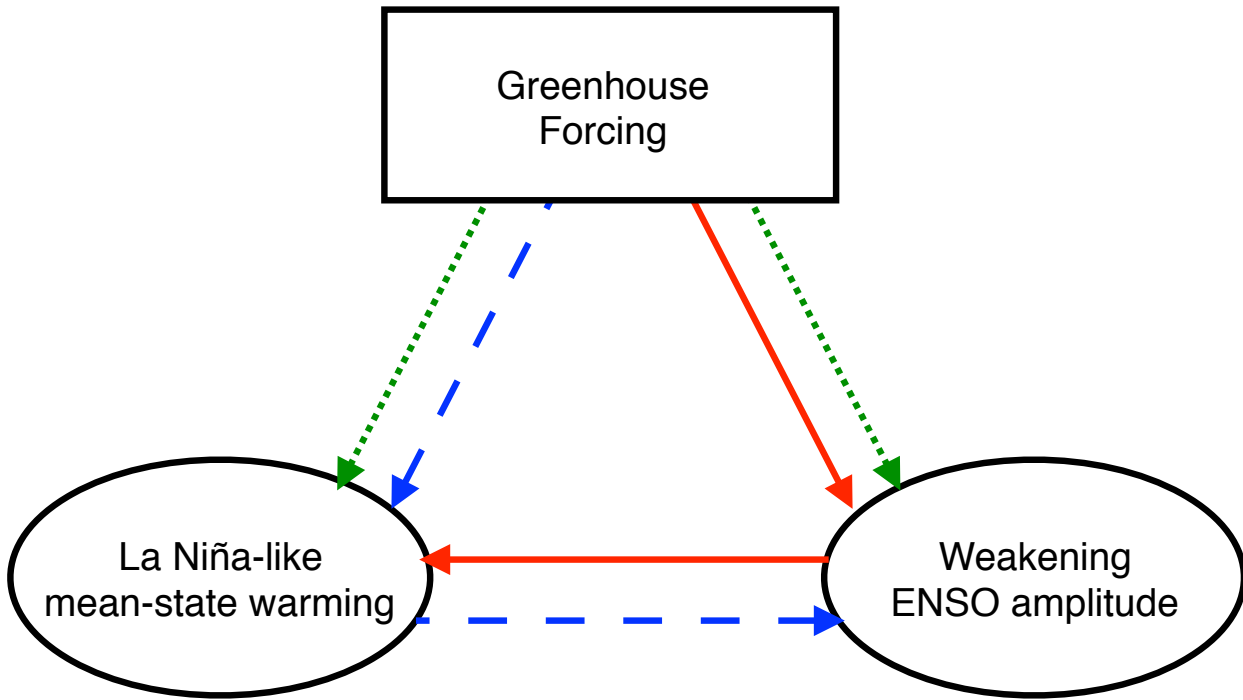
603 FIG. 6. (a): With-trend 3-year running standard deviations (RSTD) of the Niño3 SST anomalies in the three
 604 models under RCP 8.5. The dashed lines show the least-square best fit lines, and the shaded areas show the esti-
 605 mated ranges of the true trends at the 95% confidence level. (b): Detrended annual mean Niño3 SST anomalies
 606 in the three models.



607 FIG. 7. (a): Left, Detrended 3-year RSTD of the observed Niño3 SST anomalies (blue) and the zonal SST
 608 gradient (ZSG) index defined as 3-year running means of the Niño3 minus Niño4 SST anomalies (red). The
 609 results of HadISST (top) and ERA-Interim (bottom) are shown. Right, Lag correlations between the two indices
 610 shown in the left panels. Error bars show the estimated ranges of the true correlations at the 95 % confidence
 611 level. (b): As in (a), but for GFDL-ESM2M under RCP 6.0 and 8.5. (c): As in (a), but for GFDL-ESM2G and
 612 HadGEM2-CC under RCP 8.5.

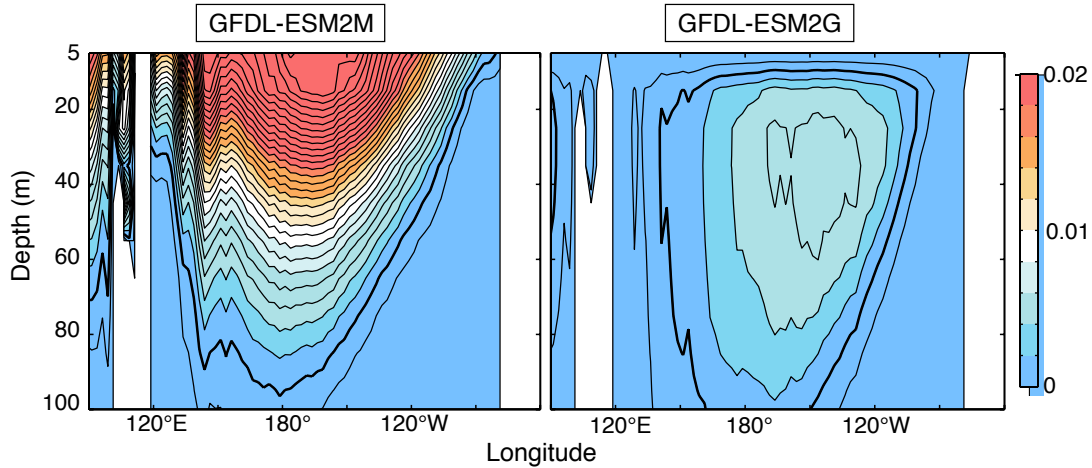


613 FIG. 8. (a): As in the left panels in Fig. 7, but the window length is 7 years. Only the results of HadISST and
 614 GFDL-ESM2M (RCP 6.0 and 8.5) are shown. Correlation coefficients are shown at the top right. For RCP 8.5,
 615 also shown is the same plot but for the with-trend indices. The dashed lines show the least-square best fit lines.
 616 (b): As in (a), but the window length is 11 years.

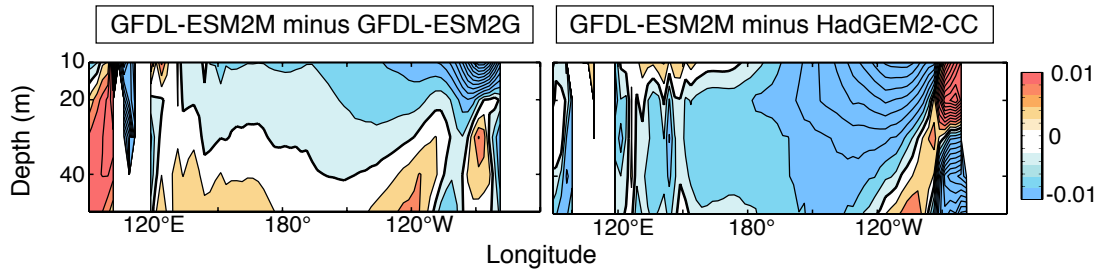


617 FIG. 9. Three possible causal relationships among greenhouse forcing, the ENSO amplitude change, and the
 618 La Niña-like mean-state response in GFDL-ESM2M.

a) Equatorial vertical heat diffusivity

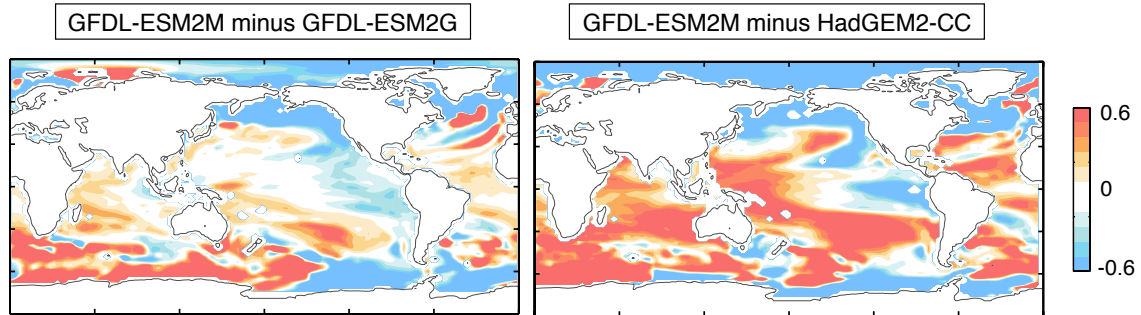


b) Equatorial Thermal Stratification

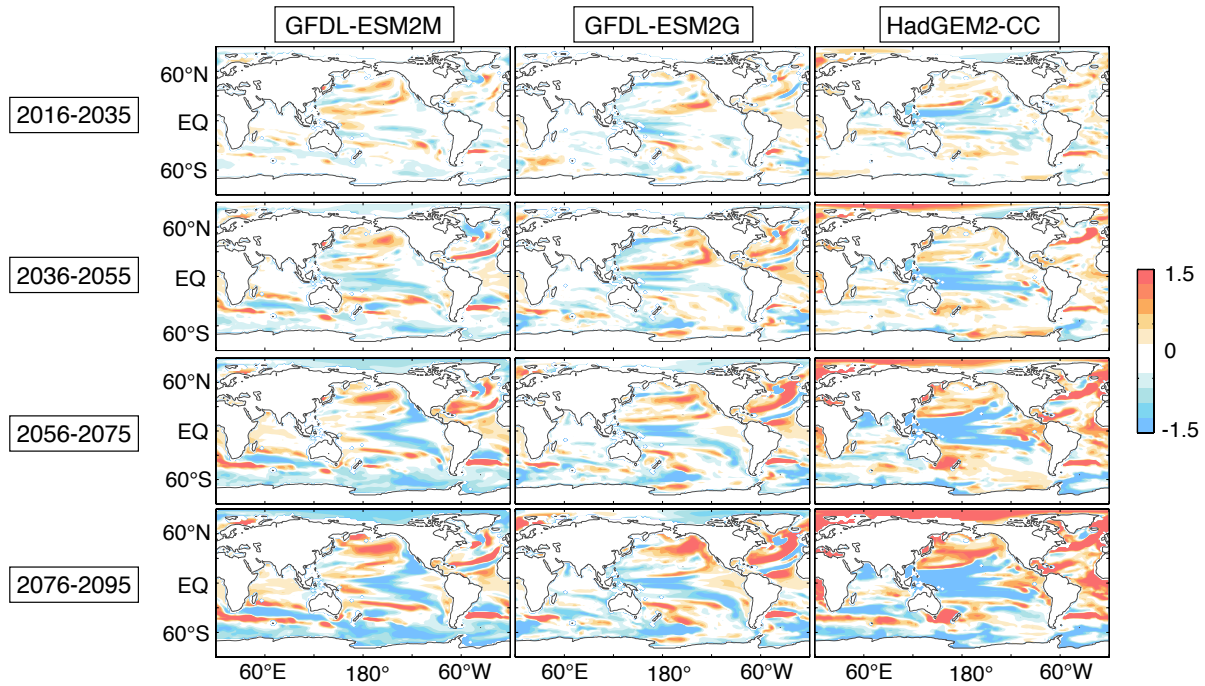


619 FIG. 10. (a): Climatology of the equatorial (5°S - 5°N) vertical heat diffusivity in the two models derived from
 620 historical runs. Bold lines show $0.002 \text{ m}^2/\text{s}$, contour interval is $0.001 \text{ m}^2/\text{s}$, and higher diffusivity is shaded
 621 orange. (b): Difference of the climatological, equatorial thermal stratification between GFDL-ESM2M and the
 622 other two models derived from 2006-2035 in the RCP 8.5 runs. Bold lines show 0 /s , contour interval is 0.004
 623 /s , and positive (negative) values are shaded orange (blue).

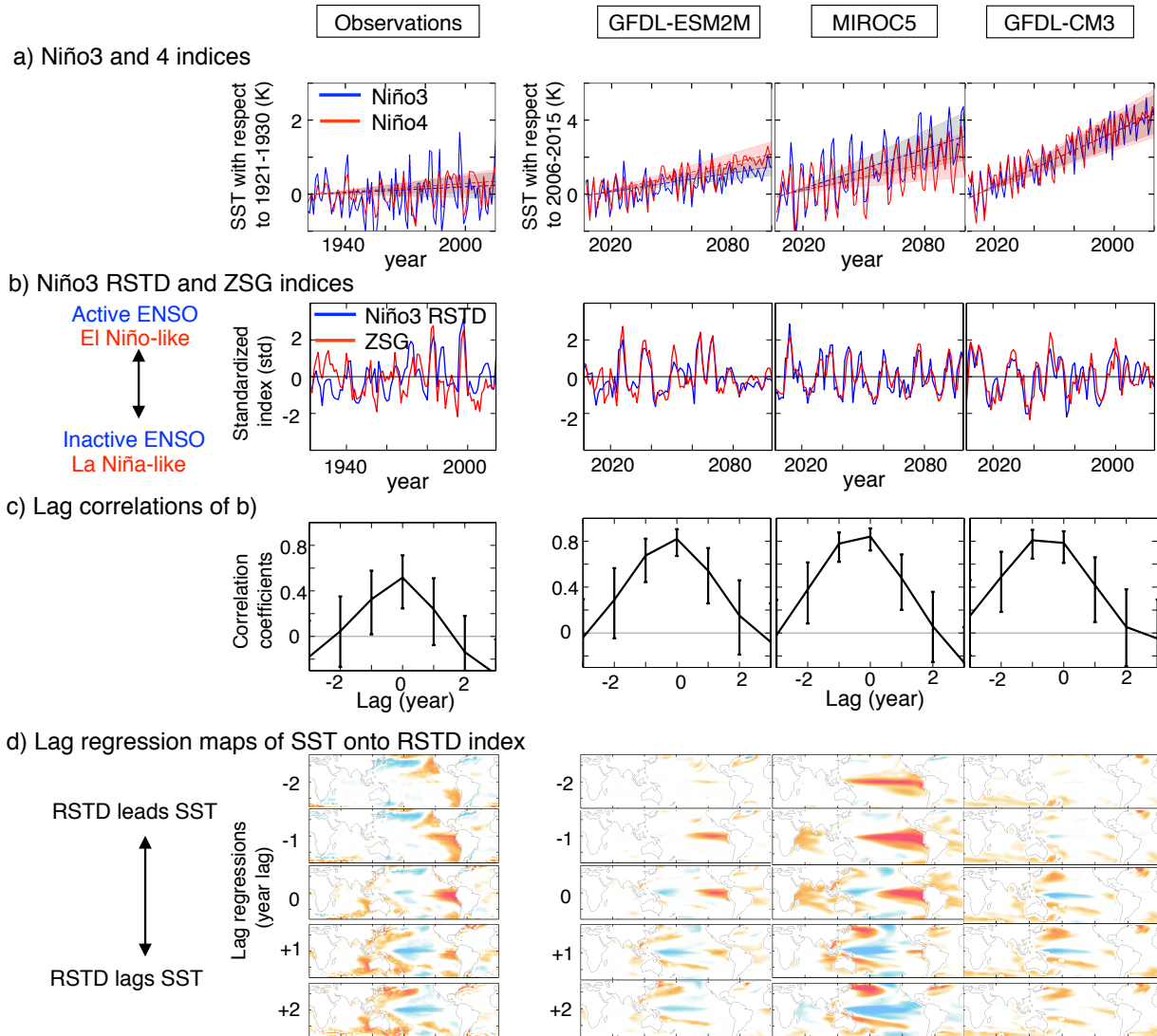
a) Strength of the polar amplification



b) Oceanic warming averaged over the 150-200 m layer



624 FIG. 11. (a): Difference of the SST* warming response between GFDL-ESM2M and the other two models.
 625 The warming response is calculated as epochal difference of 2071-2100 minus 2006-2035. (b): As in Fig. 2, but
 626 for the vertical mean oceanic temperature within the 150-200 m layer.



627 FIG. 12. (a): The annual mean Niño3 (blue) and Niño4 (red) SST anomalies expressed with respect to 1921-
 628 1930 (observations) or 2006-2015 (models). Observations are from HadISST, and the model outputs are derived
 629 from RCP 8.5. Dashed lines show the least-square best fit lines, and the shaded areas show the estimated ranges
 630 of the true trends. (b): As in the left panels in Fig. 7, but for observations and a different set of three models
 631 under RCP 8.5. The plots of observations and GFDL-ESM2M are identical as ones shown in Fig. 7. (c): As in
 632 (b), but for the right panels in Fig. 7. (d): Lag regression maps of detrended annual mean SST onto detrended
 633 3-year RSTD of the Niño3 SST anomalies. Each row shows different lags. The positive lags denote that RSTD
 634 lags SST, and vice versa. Positive (negative) anomalies are shaded orange (blue).